Something something something physics

Steven Green
of Emmanuel College

A dissertation submitted to the University of Cambridge
for the degree of Doctor of Philosophy

Abstract

This thesis describes the optimisation of the calorimeter design for collider experiments at the future Compact LInear Collider (CLIC) and the International Linear Collider (ILC). The detector design of these experiments is built around high-granularity Particle Flow Calorimetry that, in contrast to traditional calorimetry, uses the energy measurements for charged particles from the tracking detectors. This can only be realised if calorimetric energy deposits from charged particles can be separated from those of neutral particles. This is made possible with fine granularity calorimeters and sophisticated pattern recognition software, which is provided by the PandoraPFA algorithm. This thesis presents results on Particle Flow calorimetry performance for a number of detector configurations. To obtain these results a new calibration procedure was developed and applied to the detector simulation and reconstruction to ensure optimal performance was achieved for each detector configuration considered.

This thesis also describes the development of a software compensation technique that vastly improves the intrinsic energy resolution of a Particle Flow Calorimetry detector. This technique is implemented within the PandoraPFA framework and demonstrates the gains that can be made by fully exploiting the information provided by the fine granularity calorimeters envisaged at a future linear collider.

A study of the sensitivity of the CLIC experiment to anomalous gauge couplings that effect vector boson scattering processes is presented. These anomalous couplings provide insight into possible beyond standard model physics. This study, which utilises the excellent jet energy resolution from Particle Flow Calorimetry, was performed at centre-of-mass energies of 1.4 TeV and 3 TeV with integrated lumi-

nosities of 1.5ab^{-1} and 2ab^{-1} respectively. The precision achievable at CLIC is shown to be approximately one to two orders of magnitude better than that currently offered by the LHC.

Finally, a study into various technology options for the CLIC vertex detector is described.

Declaration

This dissertation is the result of my own work, except where explicit reference is made to the work of others, and has not been submitted for another qualification to this or any other university. This dissertation does not exceed the word limit for the respective Degree Committee.

Andy Buckley

Acknowledgements

Of the many people who deserve thanks, some are particularly prominent, such as my supervisor…

Preface

This thesis describes my research on various aspects of the LHCb particle physics program, centred around the LHCb detector and LHC accelerator at CERN in Geneva.

For this example, I'll just mention Chapter **??** and Chapter **??**.

Contents

“Writing in English is the most ingenious torture ever devised for sins committed in previous lives.”

— James Joyce

Chapter 1

The sensitivity of CLIC to anomalous gauge couplings through vector boson scattering

"Kids, you tried your best, and you failed miserably. The lesson is, never try."
— Homer Simpson

1.1 Motivation

Vector boson scattering is the interaction of the form VV $\rightarrow$ VV where V is any of the electroweak gauge bosons W^+, W^-, Z or γ. This is an interesting process to look at because it gives a detailed understanding of how the standard model Higgs is able to unitarise the otherwise unbounded cross section for longitudinal gauge boson scattering. Vector boson scattering also provides insights into beyond standard model physics that impacts the electroweak sector through the probing of anomalous triple and quartic gauge couplings. Presented in this section is an analysis into the sensitivity of CLIC to two of these anomalous quartic gauge couplings through the vector boson scattering process.

Triple and quartic gauge couplings lead to interactions of the form V $\rightarrow$ VV and VV $\rightarrow$ VV respectively. In the standard model there are five permissible vertices, shown in figure 1.1, which arise from the kinematic term $\mathcal{L}_{kin} = -\frac{1}{4}B_{\mu\nu}B^{\mu\nu} - \frac{1}{4}W_{\mu\nu}W^{\mu\nu}$.

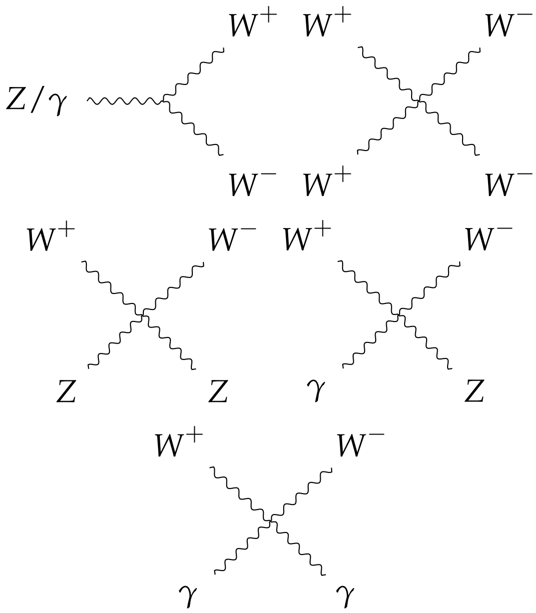

Figure 1.1: Gauge boson self-coupling vertices in the standard model.

Anomalous triple and quartic gauge couplings are introduced as parameters in effective field theory models (EFTs). These anomalous couplings can either modify the standard model triple and quartic gauge boson couplings or introduce new triple and quartic couplings that were previously forbidden.

EFT models work under the assumption than new physics exists at an energy scale, Λ that is much higher than the energy scales currently accessible to modern day particle physics experiments. Furthermore, in limit $\Lambda \to \infty$ the standard model should be reproduced as the new physics becomes kinematically inaccessible. Such theories are also model independent, giving them a wide span in the search for new physics.

A classic example of an EFT theory is the Fermi theory for beta decay. The weak interaction occurring when a neutron decays into a proton, electron and anti-neutrino can be, at energies much below the mass of the W boson, can be treated as a four-point vertex with quartic coupling strength G_F, the Fermi Coupling constant. (Feynamn Diagram if keep)

This analysis examines the anomalous quartic gauge couplings α_4 and α_5, which are introduced as part of an EFT described in chapter **??**. They appear in the Lagrangian through the following terms

$$\alpha_4[\mathrm{Tr}(V^\mu V_\mu)]^2 \text{ and } \alpha_5 \mathrm{Tr}(V^\mu V_\nu)]\mathrm{Tr}(V^\nu V_\mu)], \tag{1.1}$$

where V_μ corresponds, in a carefully chosen gauge, to a linear combination of the massive gauge bosons W^+, W^- and Z. These terms affect the coupling constants for the standard model vertices $W^+W^- \rightarrow W^+W^-$ and $W^+W^- \rightarrow ZZ$ as well as introducing the new vertex $ZZ \rightarrow ZZ$. Vector boson scattering was an appropriate process to consider for a sensitivity study into the anomalous gauge couplings α_4 and α_5 as quartic gauge boson self-interaction vertices will be present in the dominant channels for such interactions (FEYNMAN DIAGRAM).

As CLIC is purposefully deigned for high precision measurements it is ideal for a study into vector boson scattering. The application of Particle Flow Calorimetry with fine granularity calorimeters gives CLIC excellent jet energy resolution, which allows it to clearly characterise the multi-jet final states. When considering the invariant mass of these paired up jets, the nominal jet energy resolution for CLIC allows for accurate separation of W and Z bosons, which will be invaluable for event selection. This precision also helps CLIC to characterise final states containing missing energy in the form of neutrinos. The cross sections for the relevant processes are sufficiently large at the proposed running energies for CLIC to give a large sample size for this analysis. Finally, this study offers the potential to give results several orders of magnitude better than the complementary studies at the LHC due to the reduction in hadronic backgrounds and the high $\sqrt{s}$ for the interaction offered by colliding leptons instead of protons. All of the above reasons make a strong case for performing this analysis at CLIC.

This study focuses on determining the sensitivity of CLIC to the anomalous gauge couplings based solely upon the vector boson scattering processes where the outgoing bosons decay purely hadronically. This decision was made as the hadronic channels are the dominant decay modes of the W and the Z boson, with branching fractions of the order of 70% for both [3], and given CLIC has excellent jet energy resolution . Therefore, the signal final states in this analysis are the following: $\nu\nu$qqqq, lνqqqq and llqqqq. Feynman diagrams involving vector boson scattering with these final states are shown in figure 1.2.

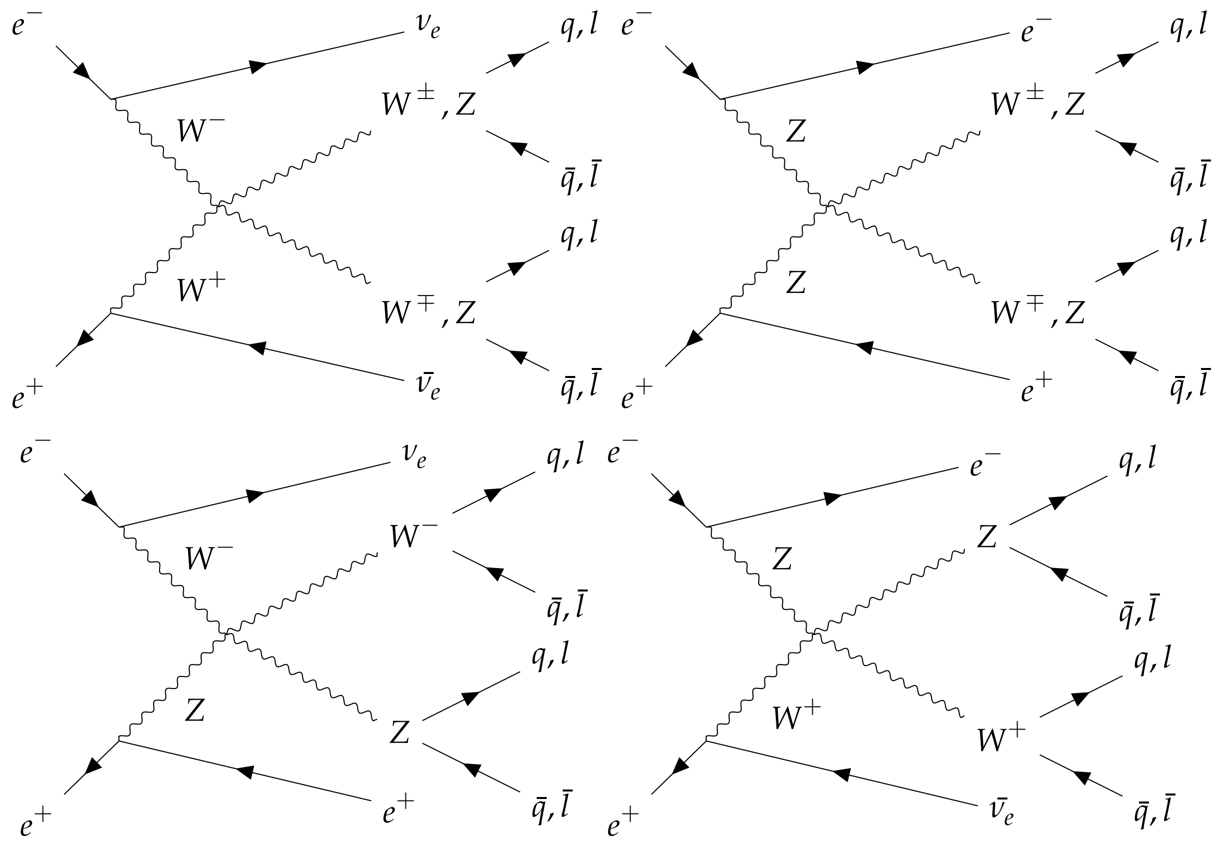

Figure 1.2: Feynman diagram of vector boson scattering at CLIC. $q = \mathrm{u, d, s, b, c}$ and $l = \mathrm{e}, \mu, \tau, \nu_e, \nu_\nu, \nu_\tau$

1.2 Event Generation, Simulation and Reconstruction

Check this doesn't sound too close to Higgs paper.

Events were generated for this analysis using the Whizard [8,12] 1.95 program. Due to the presence of beamstrahlung photons in the CLIC beam events were generated from collisions of $\mathrm{e^+e^-}$, $\mathrm{e^+}\gamma$, $\gamma\mathrm{e^-}$ and $\gamma\gamma$. The energy spectra used for all particles involved in these collisions accounted for the effects of radiation in the form of beamstrahlung photons and the intrinsic energy spread of the CLIC beam. Furthermore, events involving the interaction between the electromagnetic field of the beam particles involving quasi-real photon mediators with low momenta, described by the Weizsacker-Williams approximation or the Equivalent Photon Approximation (EPA), were generated using Whizard and included in this analysis. Fragmentation and hadronisation was implemented using PYTHIA 6.4 [13], which was tuned for OPAL e^+e^- collision data recorded at LEP (see [9] for details). The decays of tau leptons was simulated using Tauola [15]. The full list of events simulated for this analysis, along with their standard model cross section at 1.4 TeV can be found in table 1.1. The samples generated comprise all final states that would be relevant, either as signal or background processes, for an analysis involving the purely hadronic decay channels involved in a vector boson scattering process. In full they are:

- Vector boson scattering signal final states that are expected to show sensitivity to the anomalous couplings: $e^+e^- \to \nu\nu qqqq$, $e^+e^- \to l\nu qqqq$ and $e^+e^- \to llqqqq$
- Four jet final states arising from e^+e^- interactions: $e^+e^- \to qqqq$.
- Two jet final states arising from e^+e^- interactions: $e^+e^- \to \nu\nu qq$, $e^+e^- \to l\nu qq$, $e^+e^- \to llqq$ and $e^+e^- \to qq$.
- Four jet final states arising from the interactions of either e^+ or e^- with a beamstrahlung photon: $\gamma_{BS}e^- \to qqqqe^-$, $e^+\gamma_{BS} \to qqqqe^+$, $\gamma_{BS}e^- \to qqqq\nu$ and $e^+\gamma_{BS} \to qqqq\nu$.
- Four jet final states arising from the interactions of either e^+ or e^- with the electromagnetic field of the opposing beam particle. These cross sections are calculated using the EPA approximation, which represents the electromagnetic field of the opposing beam particle as a series of photons, so the final states appear as interactions of e^+ or e^- with photons: $\gamma_{EPA}e^- \to qqqqe^-$, $e^+\gamma_{EPA} \to qqqqe^+$, $\gamma_{EPA}e^- \to qqqq\nu$ and $e^+\gamma_{EPA} \to qqqq\nu$.
- Four jet final states arising from the interaction of the electromagnetic fields of opposing beam particles using the EPA approximation: $\gamma_{EPA}\gamma_{EPA} \to qqqq$.
- Four jet final states arising from the interaction of the electromagnetic field of either e^+ or e^- using the EPA approximation with a beamstrahlung photon: $\gamma_{EPA}\gamma_{BS} \to qqqq$ or $\gamma_{BS}\gamma_{EPA} \to qqqq$.
- Four jet final states arising from the interaction of two beamstrahlung photons: $\gamma_{BS}\gamma_{BS} \to qqqq$.

In the above list q represents u, $\bar{u}$, d, $\bar{d}$, s, $\bar{s}$, c, $\bar{c}$, b or $\bar{b}$; l represents $e^\pm$, $\mu^\pm$ or $\tau^\pm$; and ν represents ν_e, $\overline{\nu_e}$, ν_μ, $\overline{\nu_\mu}$, ν_τ and $\overline{\nu_\tau}$

The samples used in this analysis were simulated with the CLID_ILD detector model [1]. The simulation was performed in MOKKA [11], a GEANT4 [2] wrapper providing detailed geometric descriptions of detector concepts for the linear collider. Events were reconstructed using MARLIN [6], a c++ framework designed for reconstruction at the linear collider. PandoraPFA [10,14] was used to apply Particle Flow Calorimetry in the reconstruction, the full details of which can be found in chapter PANDORA CHAPTER.

The CLIC_ILD is a variant of the ILD detector described in section REFERENCE. The only significant difference between the models is that CLIC_ILD has a 60 layer scintillator-tugsten HCal in comparison to the 48 layers found in the default ILD detector. The thicknesses of the layers in the HCal models are identical, so the extra layers correspond to an increase in the total thickness of the HCal. This is needed to compensate for the effects of leakage at the higher energies seen by the CLIC experiment in comparison to the ILC.

1.3 Modelling of Anomalous Gauge Couplings

It was necessary when generating samples that are sensitive to the anomalous gauge couplings α_4 and α_5 to use Whizard version 1.97, instead of the previously quoted version 1.95. This change was required as version 1.97 contained a unitarisation scheme that ensured cross sections for processes involving longitudinal gauge boson scattering were bound at the energies considered i.e. the TeV scale.

The sensitivity of an individual event to the anomalous gauge couplings is determined through an event weight. This weight is given by the ratio of the squares of the matrix element used in the cross section calculation, one matrix element using non-zero values of α_4 and α_5 and the other matrix element using the standard model values of α_4 and α_5, i.e. 0. The weight varies as a function of α_4 and α_5 as well as varying on an event by event basis as the kinematics of the final state changes. Examples of the event weights as a function of α_4 and α_5 for selected events is shown in figure 1.3 for 1.4 TeV $\nu\nu$qqqq final state events.

This reweighting procedure has many advantages over the alternative of generating new samples with fixed α_4 and α_5, notably the absence of systematic errors arising from new event generation, simulation and reconstruction. Only final states showing

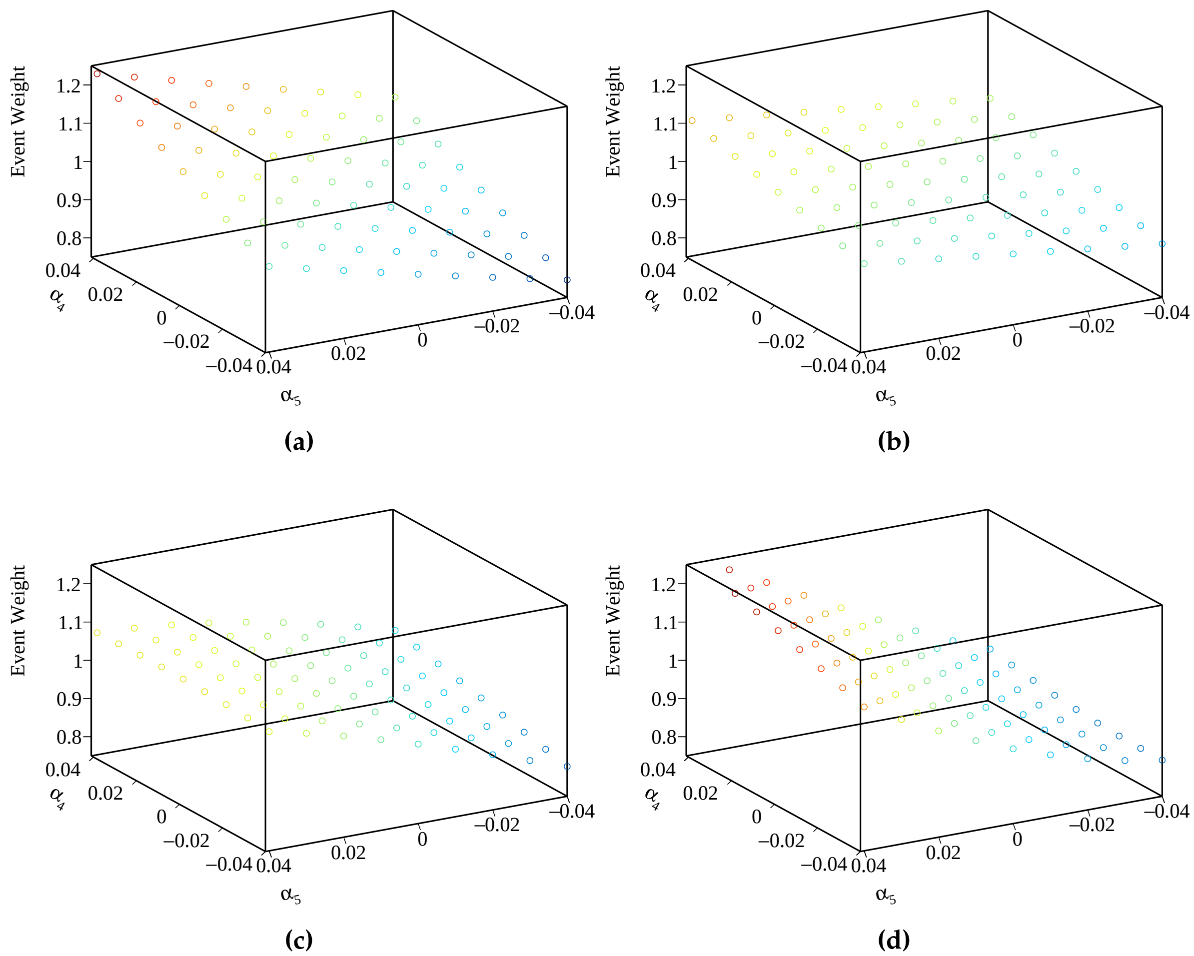

Figure 1.3: The event weight as a function of the anomalous couplings α_4 and α_5 for a selection of $\nu\nu$qqqq final state events at 1.4TeV.

Final State	Cross Section 1.4 TeV [fb]
$e^+e^- \to \nu\nu qqqq$	24.7
$e^+e^- \to l\nu qqqq$	110.4
$e^+e^- \to llqqqq$	62.1
$e^+e^- \to qqqq$	1245.1
$e^+e^- \to \nu\nu qq$	787.7
$e^+e^- \to l\nu qq$	4309.7
$e^+e^- \to llqq$	2725.8
$e^+e^- \to qq$	4009.5
$\gamma_{EPA}e^- \to qqqqe^-$	287.1
$\gamma_{BS}e^- \to qqqqe^-$	1160.7
$e^+\gamma_{EPA} \to qqqqe^+$	286.9
$e^+\gamma_{BS} \to qqqqe^+$	1156.3
$\gamma_{EPA}e^- \to qqqq\nu$	32.6
$\gamma_{BS}e^- \to qqqq\nu$	136.9
$e^+\gamma_{EPA} \to qqqq\nu$	32.6
$e^+\gamma_{BS} \to qqqq\nu$	136.4
$\gamma_{EPA}\gamma_{EPA} \to qqqq$	753.0
$\gamma_{EPA}\gamma_{BS} \to qqqq$	4034.8
$\gamma_{BS}\gamma_{EPA} \to qqqq$	4018.7
$\gamma_{BS}\gamma_{BS} \to qqqq$	21406.2

Table 1.1: Cross sections of signal and background processes at 1.4 TeV. In the above table q represents u, ū, d, d̄, s, s̄, c, c̄, b or b̄; l represents $e^{\pm}$, $\mu^{\pm}$ or $\tau^{\pm}$; and ν represents ν_e, $\overline{\nu_e}$, ν_μ, $\overline{\nu_\mu}$, ν_τ and $\overline{\nu_\tau}$. The EPA and BS subscript on the incoming photon indicates whether the photon is generated from the equivalent photon approximation or beamstrahlung.

a sensitivity to α_4 and α_5 require reweighting. To determine those states a comparison was made between the cross section using the standard model values of α_4 and α_5, i.e. 0, and the same calculation using non-zero values of these couplings at 1.4 TeV. This comparison was performed on all of the generated samples listed in table 1.1 and the results for samples showing sensitivity to the couplings can be found in table 1.2

The cross sections were found to differ when using non-zero values for the anomalous couplings in comparison to the standard model prediction only for the vector boson scattering signal final states $\nu\nu qqqq$, $l\nu qqqq$ and $llqqqq$. In reality, non-zero anomalous couplings would change the cross sections of all processes considered; however, the sensitivity would only arise from high order terms in the Lagrangian. Such terms would not be dominant in determining the cross section and so are omitted from the generator making certain final states appear invariant to changes in the anomalous couplings.

Final State	Cross Section [fb] ($\alpha_4 = \alpha_5 = 0.00$)	Cross Section [fb] ($\alpha_4 = \alpha_5 = 0.05$)	Percentage Change[%]
$e^+e^- \rightarrow \nu\nu qqqq$	24.7	34.6	+40.1
$e^+e^- \rightarrow l\nu qqqq$	115.3	113.0	-2.0
$e^+e^- \rightarrow llqqqq$	62.1	68.6	+10.5

Table 1.2: Cross sections for selected processes showing the effect of the anomalous gauge couplings α_4 and α_5 at 1.4 TeV.

The cross section calculations show that the most sensitive final state to the anomalous gauge couplings is $\nu\nu$qqqq; therefore, this analysis will focus entirely upon this final state. Furthermore, as the lνqqqq final state has a much reduced sensitivity in comparison to the $\nu\nu$qqqq state and as the llqqqq can be easily vetoed from the analysis, as will be shown in subsequent chapters, it is only necessary to consider the sensitivity of the $\nu\nu$qqqq final state. For the aforementioned reasons the lνqqqq and llqqqq final states will be treated as backgrounds that are invariant to changes in the anomalous couplings α_4 and α_5.

In order to determine the anomalous gauge coupling sensitive event weights it was necessary to use the anomalous gauge coupling model in Whizard, which enforces a unit CKM matrix. In the context of vector boson scattering and the $\nu\nu$qqqq final state, which is the only final state requiring reweighting, this restricts the decays of the W^- boson to $d\bar{u}$ and $s\bar{c}$, the W^+ boson to $u\bar{d}$ and $c\bar{s}$ and the Z boson to $u\bar{u}$, $d\bar{d}$, $s\bar{s}$, $c\bar{c}$ and $b\bar{b}$. In comparison, the non-unit CKM matrix allows for extra decay modes, however, this was found to have a negligible effect on the samples when comparing several reconstructed level distributions. Furthermore, flavour tagging of jets was not used in this analysis as it offered negligible gains when performing event selection.

1.4 Data Analysis

The focus of this section is to describe the post reconstruction procedure applied to the signal and background events, described in **??**, to extract the relevant information needed for this sensitivity study.

1.4.1 Jet Finding

After the reconstruction two further processors are applied to remove reconstructed particle flow objects (PFOs) that originate from beam related backgrounds, described in section CLIC BEAM CHAPER, from the event. The first processor is the CLICTrack-Selection, designed to veto poorly reconstructed tracks and to reject tracks where the time of arrival at the calorimeter between the helix fit to the track and to a straight line of flight differ by 50ns. The latter would indicate the tracked particle does not create the calorimetric energy deposits that it has been associated to. The second processor is the CLICPfoSelector, which applies cuts to the p_{T} and timing information of the PFOs. These cuts vary as a function of position in the detector and the reconstructed particle type in an attempt to target the regions of the detector where background, primarily low p_{T} $\gamma\gamma \rightarrow$ Hadrons events, are more prominent. Three configurations of the CLICPfoSelector have been developed for the CLIC environment and were considered for this analysis. They are, in order of increasing background rejection, the Loose, Default and Tight selections. The full details of each can be found here [10].

After the application of the CLICTrackSelection and CLICPfoSelector the MarlinFastJet processor, a wrapper for the FastJet [5] processor, was used to cluster the events into four jets. These jets are then paired up to form two candidate bosons. This pairing is performed on the assumption that the correct pairing is achieved when the difference between the invariant masses is a minima. In the case of the signal final state, $\nu\nu$qqqq, it is assumed that the four jets and two candidate bosons map onto the four quarks and the two outgoing bosons involved in the vector boson scattering process. The jet clustering was done using the longitudinally invariant k_t jet algorithm in exclusive mode. In contrast to the inclusive mode, the exclusive mode allows the user to request a fixed number of jets in the output from MarlinFastJet. The longitudinally invariant k_t algorithm proceeds as follows:

- For each pair of particles, i and j, the k_t distance, d_{ij}, and beam distance, $d_{iB} = p_t^2$, was calculated.

$$d_{ij} = \min(p_{ti}^2, p_{tj}^2)\Delta R_{ij}^2/R^2 \tag{1.2}$$

  where $\Delta R_{ij}^2 = (y_i - y_j)^2 + (\phi_i - \phi_j)^2$, p_t is the transverse momentum of the particle with respect to the beam axis, y_i is the rapidity of particle i and ϕ_i is the azimuthal angle of particle i. R is a configurable parameter that typically is of the order of 1.

- The minimum distance, $d_{\min}$, of all the k_t and beam distances was found. If the minimum occurrs for a k_t distance, particles i and j were merged, summing their 4-momenta. If the beam distance was the minima, particle i was declared to be part of the "beam" jet. The particle was removed from the list of particles and not included in the final jet output.

- This was repeated until the desired number of jets was created. Alternatively, in inclusive mode this would be repeated until no particles are left in the event.

Two other clustering algorithms were considered, but, as figure 1.4 shows, were found to be inappropriate for the experimental conditions at CLIC. These alternative algorithm choices are applied in the same manor as the longitudinally invariant k_t algorithm, however, they differ in the definition of the k_t distance, d_{ij}, and the beam distance, d_{iB}.

The first alternative jet algorithm considered was the k_t algorithm for e^+e^- colliders, the EE_kt or Durham algorithm, where $d_{ij} = 2\min(E_i^2, E_j^2)(1 - cos\theta_{ij})$ and d_{iB} is not used. θ_{ij} is the opening angle of particles i and j meaning that in the collinear limit d_{ij} corresponds to the relative transverse momenta of the particles. The major failure of this algorithm when applied to CLIC is the absence of d_{iB}, which leads to many beam related background particles being associated to jets. As figure 1.4 shows, the invariant mass of the paired jets, which should peak around the W and Z boson masses, is much larger than expected, due to the presence of the beam related backgrounds in the jets. Also this algorithm is not invariant to boosts along the beam direction making it inappropriate to use at CLIC as the beam induced backgrounds modify the nominal collision kinematics.

The second alternative jet algorithm considered was the Cambridge-Aachen jet algorithm where $d_{ij} = \Delta R_{ij}^2/R^2$ and $d_{iB} = 1$. This algorithm performed poorly as neither accounts for the transverse momentum nor energy of the particles being clustered. In essence, this is a cone clustering algorithm with a cone radius defined through $\Delta R_{ij} = R$, which even for large R was found to discard too much energy in the event to be useful for this analysis. This can be seen in figure 1.4 as the invariant mass of the paired jets is much lower than expected. This algorithm is useful for events with highly boosted jets, but at CLIC the jets are too disperse for this algorithm to be successfully applied.

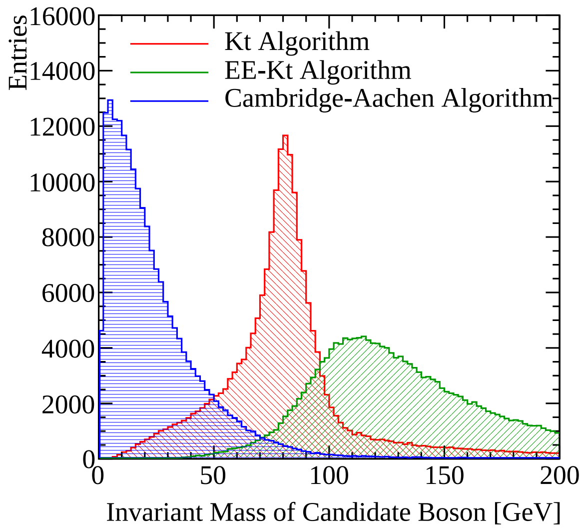

(a)

Figure 1.4: The reconstructed masses for different choices of jet algorithm for 1.4 TeV $\nu\nu$qqqq final state events. The masses are calculated by forcing the reconstructed event into 4 jets and then pairing the jet pairs to form candidate bosons. The jet pairing configuration is determined by pairing jets such that the mass differences between the two candidate bosons is a minimum. These samples should be dominated by vector boson scattering involving pairs of W bosons and so it is expected that a peak at the W boson true mass should be observed. As this does not occur for the Cambridge-Aachen algorithm or the EE_kt algorithm they were deemed unsuitable for this analysis. In the case of the kt algorithm and the EE_kt algorithm an R parameter of 0.7 was used.

Optimal Jet Finding Algorithm

Optimisation of the jet algorithm configuration was performed on the choice of PFO selection as well as the value of the R parameter used in the longitudinally invariant k_t algorithm. The optimal configuration for the jet algorithm at 1.4 TeV was found to use default selected PFOs and an R parameter of 0.9.

This procedure involved performing the sensitivity study, described in section 1.6, using solely the $\nu\nu$qqqq signal final state. This procedure leads to the construction of a χ^2 surface from which confidence contours can be extracted in the α_4 and α_5 space. The χ^2 surface is constructed by comparing the distribution of the invariant mass of the visible system, M_{VV}, with and without the effect of the anomalous couplings α_4 and α_5. The χ^2 surface for the optimal jet configuration at 1.4 TeV using the $\nu\nu$qqqq signal final state is shown in figure 1.5a. This methodology ensured that the optimisation was done with respect to the physics of interest without having to perform the jet reconstruction for the large number of background events multiple times.

Confidence limits on the individual parameters α_4 and α_5 were determined by setting the corresponding coupling term to zero and examining the now one dimensional χ^2 distribution. A fourth order polynomial was fitted to the minima of this distribution and the one sigma confidence limit defined using $\Delta\chi^2$ of 1. $\Delta\chi^2$ is defined as the change in χ^2 with respect to the minima in the χ^2 surface. Note that for the two dimensional χ^2 surface a one sigma confidence limit is given by a $\Delta\chi^2$ of 2.28 due to the additional degree of freedom in the fit. The one dimensional χ^2 distribution for α_4 and α_5, assuming $\alpha_5 = 0$ and $\alpha_4 = 0$ respectively, for the optimal jet configuration at 1.4 TeV using the $\nu\nu$qqqq signal final state is shown in figures 1.5b and 1.5c. Using these distributions the one sigma confidence limits on α_4 are -0.0038 to 0.0047 and on α_5 are -0.0027 to 0.0030.

1.4.2 Lepton Finding

An isolated lepton finder was included in the analysis chain in an attempt to reject background final states containing leptons. As it is unlikely that isolated leptons will form via hadronisation, because all hadronisation products will be boosted along the same direction, it is likely that they originate from the primary interaction occurring at the IP. This makes the number of isolated leptons a powerful discriminating variable for discerning final states containing leptons.

The isolated lepton finder used here attempts to find whether a PFO is an electron or muon based on the calorimetric energy deposits. Cuts are then placed on the tracks associated to any PFOs, initially tagged as electrons or muons, to determine whether the tracks originate from the impact point. If the track cuts deem the PFO to have originated from the impact point, isolation cuts restricting the energy in a cone

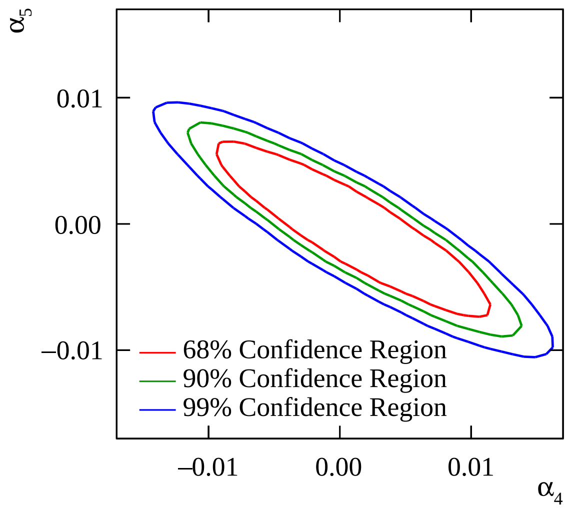

(a)

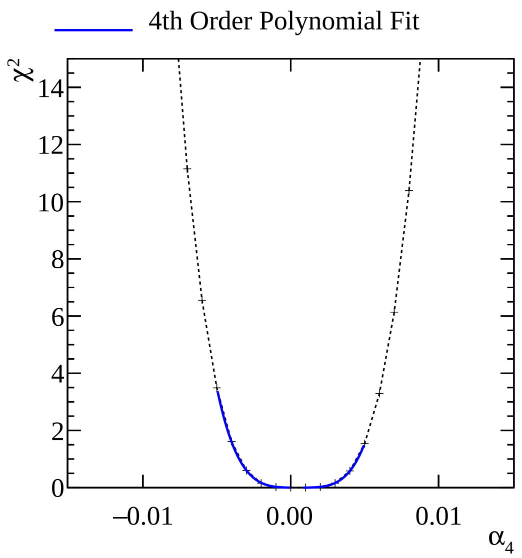

(b)

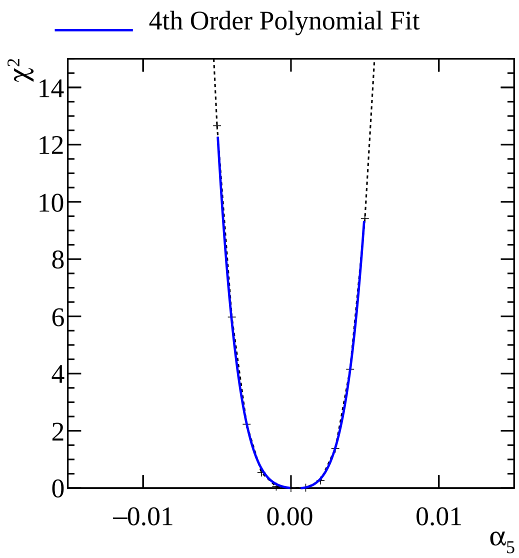

(c)

Figure 1.5: χ^2 sensitivity distributions from a fit to M_{VV} for the signal qqqq$\nu\nu$ final state only at 1.4 TeV. These results use the optimal jet algorithm configuration of selected PFOs and an R parameter of 0.9 in the k_t algorithm. (a) χ^2 sensitivity contours in α_4 and α_5 space. (b) χ^2 as a function of α_4 assuming $\alpha_5 = 0$. (c) χ^2 as a function of α_5 assuming $\alpha_4 = 0$.

surrounding these PFO are applied to ensure the particles does not belong to a jet. If a PFO passes all of these criteria then it is counted as an isolated lepton. The efficiency of the lepton finder is summarised in table 1.3.

Final State	$\epsilon_{\text{Lepton Finding}}$
$e^{+}e^{-} \rightarrow \nu\nu qqqq$	99.7
$e^{+}e^{-} \rightarrow l\nu qqqq$	48.9

Table 1.3: The efficiency of isolated lepton finding at 1.4 TeV for the $\nu\nu$qqqq and lνqqqq final states. Efficiency here is defined as the fraction of events where no isolated leptons were found.

1.4.3 Discriminant Variables

The next stage of the analysis involved the calculation of a number of event-based variables that were found to be useful for this analysis. The variables that were calculated are as follows:

- **Particle level** variables:
  - Number of PFOs in each jet.
  - Energy of the highest energy PFO.
  - Energy of the highest energy electron.
  - Cosine of the polar angle of the highest energy track.
  - The number of isolated leptons found using the isolated lepton finder.
- **Candidate boson** variables:
  - Energy of the candidate bosons.
  - Invariant mass of the candidate bosons.
  - Acolinearity of the candidate boson pair, which is defined as 180 degrees minus the opening angle of the pair of bosons in the rest frame of the detector.
- **Event based** variables:
  - The invariant mass of the visible system, M_{VV}.

– The vector sum of the transverse momentum of all PFOs in the event.

– Sphericity, defined through the sphericity tensor S^{ab}:

$$S^{ab} = \frac{\Sigma_i p_i^\alpha p_j^\alpha}{\Sigma_{i,\alpha=1,2,3} |p_{i|}^{\alpha}{}^2} \tag{1.3}$$

Where p_i are the components of the momenta of PFO i in the rest frame of the detector and the sum Σ_i runs over all particles in the event. Sphericity is defined as $\mathrm{S} = \frac{3}{2}(\lambda_2 + \lambda_3)$, where λ_i are the eigenvalues of the sphericity tensor defined such $\lambda_1 \geq \lambda_2 \geq \lambda_3$. This provides a measure of how spherical the reconstructed event topology is with isotropic events having $S \approx 1$, while two jet events have $S \approx 0$.

- **Jet clustering parameter** variables, y_{ij} where $i = 3, 4$ and $j = i + 1$. These are the smallest k_t distance found when combining j jets into i jets. The variable used in the multivariate analysis is $-\log_{10}(y_{ij})$.

1.5 Event Selection

As described in section 1.3 the signal final state in this analysis is the $\nu\nu$qqqq final state, while the backgrounds consist of all 2 and 4 jet final states that could be confused for the signal state in the reconstruction. A complete list of signal and background final states used for this analysis, alongside their standard model cross sections, can be found in table 1.1. In an attempt to isolate signal from background, an event selection procedure consisting of a set of preselection cuts followed by the application of a multivariate analysis (MVA) was applied to this data set and the full details of those are given in the following section.

1.5.1 Pre-Selection

A refined selection of the $\nu\nu$qqqq signal final state is achieved using MVA. However, to ensure efficiency in the training and application of that MVA a number of simple preselection cuts were developed that veto obvious background final states prior to the application of the MVA. These cuts were developed such that as much background as possible would be rejected, while retaining enough signal to make the analysis viable. Preselection cuts were applied to the transverse momentum, invariant mass of the visible system and the number of isolated leptons. The raw distributions of these variables is shown in figure 1.6 and based on these distributions the following cuts were applied:

- Transverse momentum of system > 100 GeV. This cut is effective due to the presence of missing energy in the form of neutrinos in the signal final state.
- Number of isolated leptons in system = 0. This cut is effective as the signal final state does not contain leptons, while numerous background final states do.

The impact of these preselection cuts can be found in table 1.4 in section 1.5.3.

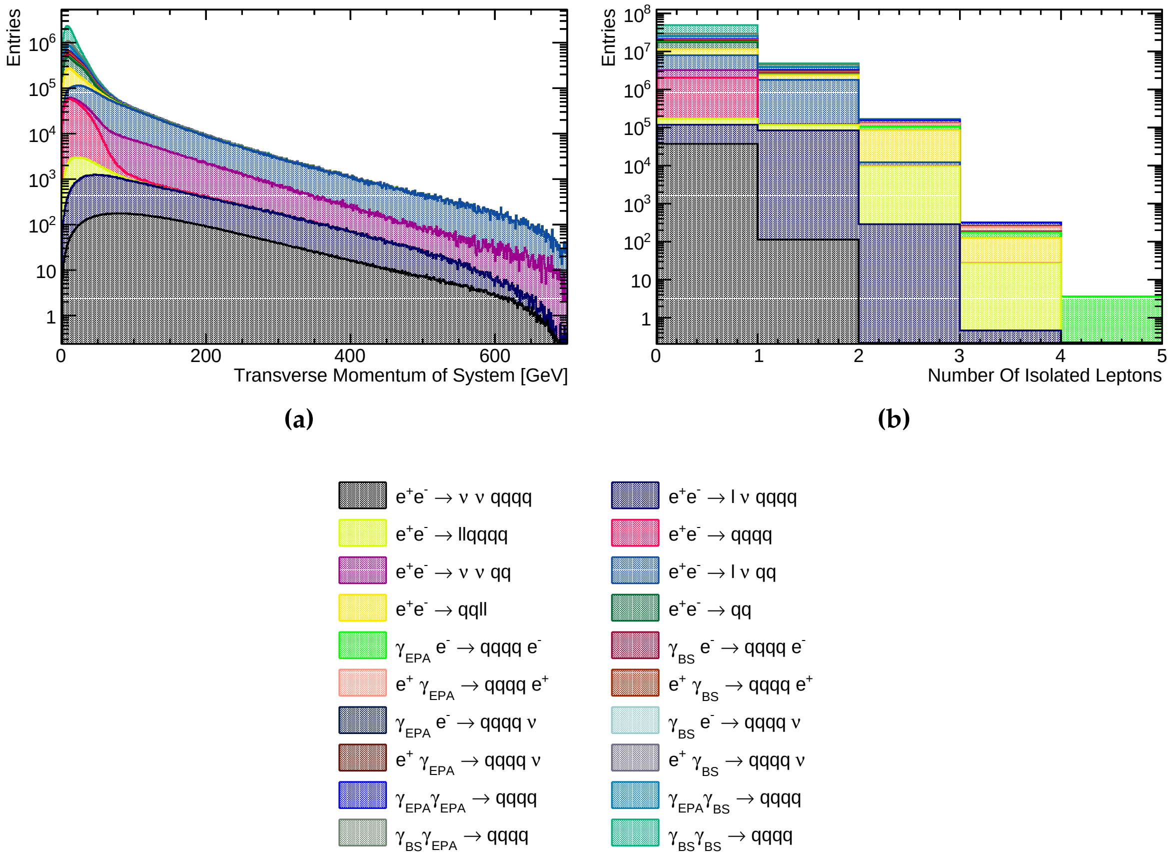

(a) **(b)** **(c)**

Figure 1.6: Distribution of variables cut on in the preselection at 1.4 TeV. (a) shows the transverse momentum of the visible system, (b) shows the number of isolated leptons in the system and (c) shows the legend for the preceding plots.

1.5.2 Multivariate analysis

Having established the preselection cuts a MVA was applied, using the TMVA toolkit [7], to refine the event selection. The signal and background final state samples were halved; one half sample was used to train the MVA and the remaining half sample was used in the subsequent analysis. The halving of the signal and background sample had minimal impact on the analysis as all event numbers were normalised to the correct luminosity for CLIC running at 1.4 TeV and the sample size was sufficiently large.

The following variables were used for training of the MVA:

- Number of PFOs in each jet.
- Energy of the highest energy PFO.
- Energy of the highest energy electron.
- Cosine of the polar angle of the highest energy track.
- Energy of the candidate bosons.
- Invariant mass of the candidate bosons.
- Acolinearity of the candidate boson pair.
- The vector sum of the transverse momentum of all PFOs in the event.
- Sphericity.
- Jet clustering parameter variables, y_{ij} where $i = 3, 4$ and $j = i + 1$. The variable used in the multivariate analysis is $-\log_{10}(y_{ij})$.

A variety of MVA options were considered and it was found that the optimal algorithm was the boosted decision tree (BDT) as shown by figure 1.7.

The BDT was further optimised by varying the number of trees used, the depth of the trees and the number of cuts applied and an optimal significance, $S/\sqrt(S+B)$, of 52.7 was obtained.

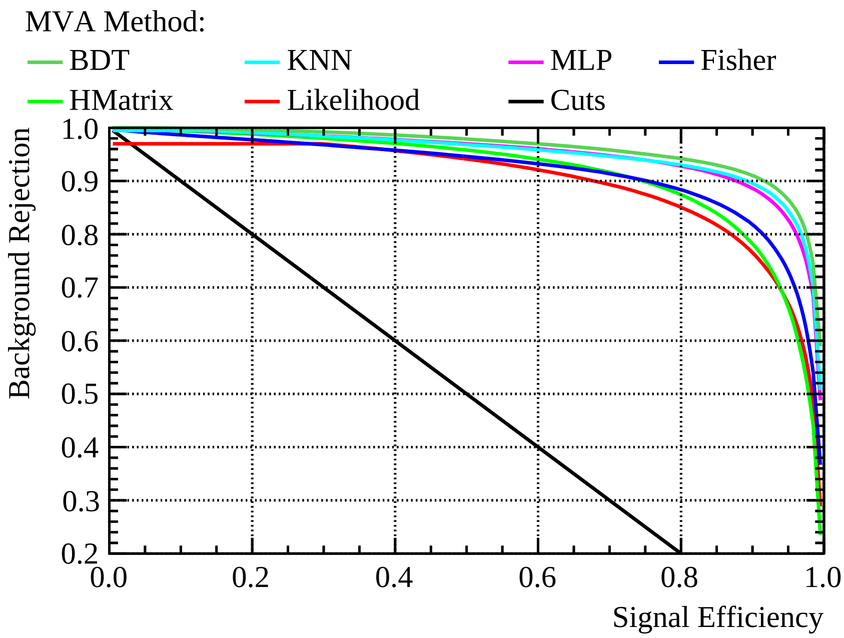

Figure 1.7: Background rejection as a function of signal efficiency for a variety of MVA options at 1.4 TeV.

1.5.3 Event Selection Summary

The event selection is summarised using the distribution of the invariant mass of the candidate bosons, which for the signal final state should peak around the W and Z masses. This distribution is shown in figure 1.8 with no event selection, with the preselection cuts and with both preselections cuts and MVA applied. The event selection is also summarised using efficiencies shown in table 1.4.

As expected the dominant background processes after the MVA is applied are those that will look identical to the visible signal process, i.e. qqqq with missing energy. Two smaller sources of background that pass the MVA exists: two jet events with missing energy, which are confused with four jet events with missing energy and those where a lepton is not properly reconstructed and the events look like four jets and missing energy.

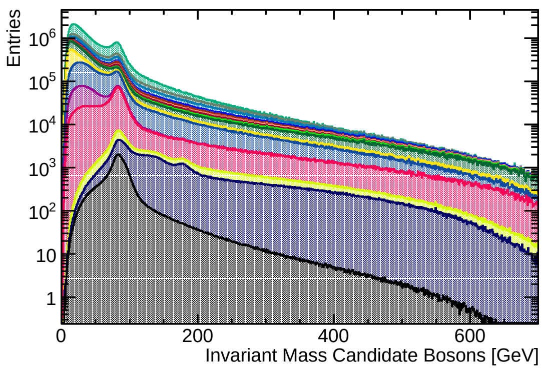

(a)

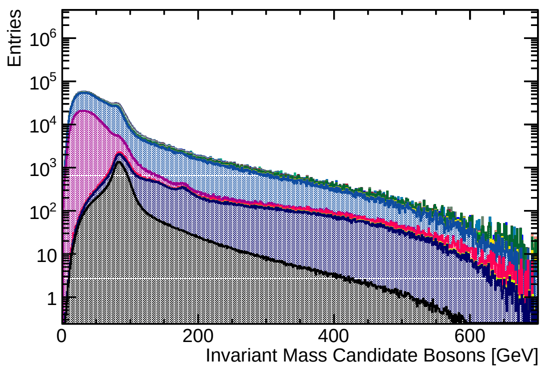

(b)

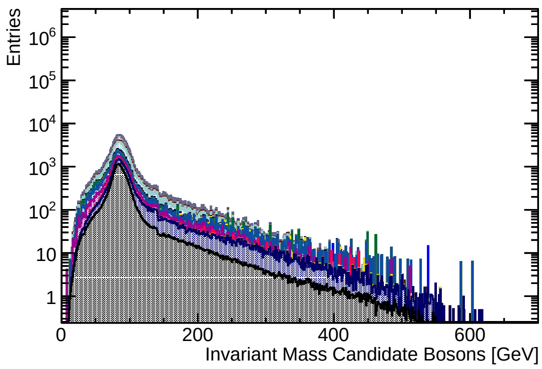

(c)

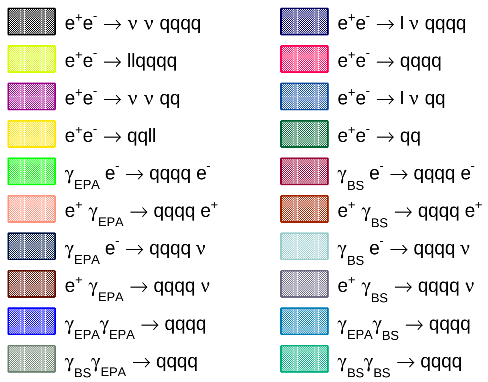

(d)

Figure 1.8: Impact of preselection and MVA on the reconstructed invariant mass of the bosons arising from jet pairing at 1.4 TeV. (b) no cuts applied. (b) preselection cuts applied. (c) MVA with preselection applied. (d) legend for the event selection plots.

Final State	ϵ_{presel}	ϵ_{BDT}	N_{BDT}
$e^+e^- \to \nu\nu qqqq$	64.1%	44.5%	16,470
$e^+e^- \to l\nu qqqq$	26.1%	5.2%	8,582
$e^+e^- \to llqqqq$	0.8%	0.1%	100
$e^+e^- \to qqqq$	0.3%	0.1%	1,698
$e^+e^- \to \nu\nu qq$	43.4%	0.5%	5,351
$e^+e^- \to l\nu qq$	19.1%	0.1%	9,319
$e^+e^- \to llqq$	0.1%	-	234
$e^+e^- \to qq$	0.6%	-	1,586
$\gamma_{\text{EPA}}e^- \to qqqqe^-$	0.2%	-	48
$\gamma_{\text{BS}}e^- \to qqqqe^-$	0.1%	-	42
$e^+\gamma_{\text{EPA}} \to qqqqe^+$	0.3%	-	19
$e^+\gamma_{\text{BS}} \to qqqqe^+$	-	-	65
$\gamma_{\text{EPA}}e^- \to qqqq\nu$	26.0%	9.0%	4,421
$\gamma_{\text{BS}}e^- \to qqqq\nu$	36.1%	15.0%	23,150
$e^+\gamma_{\text{EPA}} \to qqqq\nu$	25.9%	9.2%	4,495
$e^+\gamma_{\text{BS}} \to qqqq\nu$	36.4%	15.3%	23,410
$\gamma_{\text{EPA}}\gamma_{\text{EPA}} \to qqqq$	0.2%	-	81
$\gamma_{\text{EPA}}\gamma_{\text{BS}} \to qqqq$	0.1%	-	55
$\gamma_{\text{BS}}\gamma_{\text{EPA}} \to qqqq$	-	-	53
$\gamma_{\text{BS}}\gamma_{\text{BS}} \to qqqq$	-	-	0

Table 1.4: Selection summary at 1.4TeV. The EPA and BS subscript on the incoming photon indicates whether the photon is generated from the equivalent photon approximation or beamstrahlung. Cells omitting the efficiency indicate an efficiency of less than 0.1%.

1.6 Effect of Anomalous Coupling/Fitting Methodology

This section describes the procedure used for constructing the χ^2 surface and the subsequent confidence contours used to determine the sensitivity of CLIC to the anomalous gauge couplings α_4 and α_5.

1.6.1 Sensitive Distribution

The sensitivity of CLIC to the anomalous gauge couplings is determined through the use of a χ^2 fit to the distribution of M_{VV}, the invariant mass of the visible system. For a given event, the jet clustering and pairing proceeds as described in section **??**. This leads to each event being clustered into four jets that are then paired up to give two candidate bosons. The distribution of M_{VV} proved to be highly sensitive to the anomalous gauge couplings, particularly for at large invariant masses, as shown in figure 1.9.

Two other distributions were considered for this sensitivity study, but proved to be less sensitive than M_{VV}: $\cos\theta^*_{Jets}$, the angle between the boost direction and the back to back quark jets in the rest frame of the candidate bosons, and $\cos\theta^*_{Bosons}$, the angle between the boost direction and the back to back candidate bosons in the rest frame of the visible system. The sensitivity of these variables can be seen in figure 1.10. It should be noted that there are two entries, one from each candidate boson, in the $\cos\theta^*_{Jets}$ distribution per event. To negate the effect of correlation between these two variables when performing the χ^2 fit, a two dimensional fit of $\cos\theta^*_{Jets}$ variable was applied where a distinction between candidate bosons was made based on their energy. When this was done the sensitivity of the $\cos\theta^*_{Jets}$ variable was worse than that obtained fitting the M_{VV} variable. Not such effect was present for the $\cos\theta^*_{Bosons}$ variable as there is only a single pair of candidate bosons per event.

1.6.2 χ^2 Surface Definition

The χ^2 surface is defined through the following equation:

$$\chi^2 = \Sigma_i \frac{(O_i - E_i)^2}{E_i}, \tag{1.4}$$

where O_i is the observed, $\alpha_4 = \alpha_5 = 0$, and E_i the expected, $\alpha_4 \neq 0$ and $\alpha_5 \neq 0$, bin content for bin i in the distribution of M_{VV}. Σ_i is the sum over the bins of the M_{VV} distribution. The distribution of M_{VV} was binned using 14 bins. The first bin spanned the invariant mass range between 0 and 200 GeV, this was followed by 11 bins of width 100 GeV ranging from 200 to 1300 GeV and finally the last bin contained

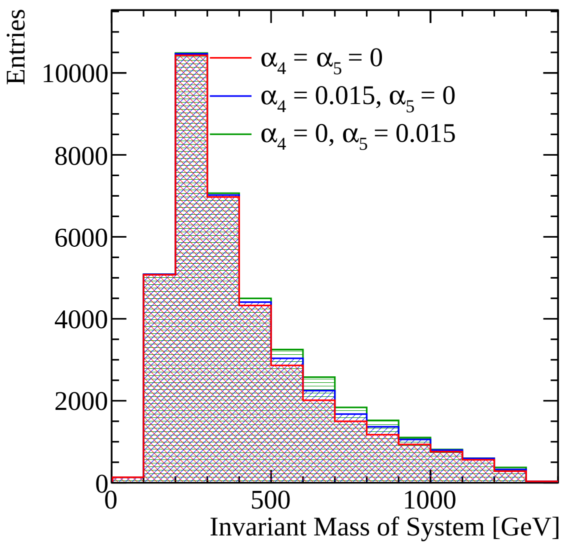

Figure 1.9: The sensitivity of M_{VV} to the anomalous gauge couplings α_4 and α_5 at 1.4 TeV. The jet algorithm used was the longitudinally invariant kt algorithm with an R parameter of 0.9 and Selected PFOs were used. This distribution is for the $\nu\nu$qqqq signal final state only.

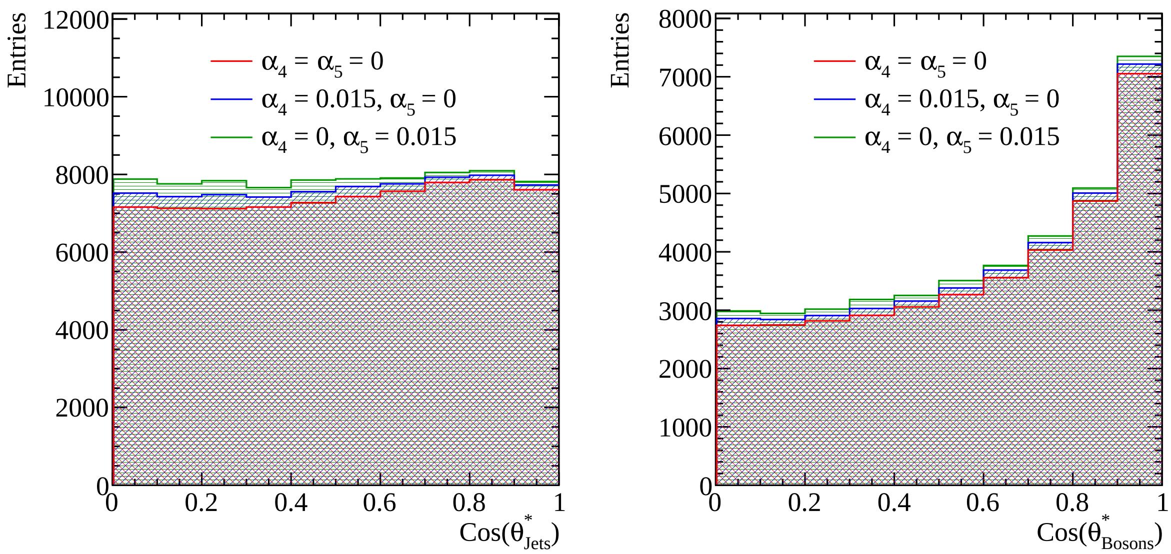

(a) **(b)**

Figure 1.10: The sensitivity of various variables to the anomalous gauge couplings α_4 and α_5 at 1.4 TeV. The jet algorithm used was the longitudinally invariant kt algorithm with an R parameter of 0.9 and Selected PFOs were used. This distribution is for the $\nu\nu$qqqq signal final state only. (a) shows the distribution of $\cos\theta^*_{Jets}$ and (b) shows the distribution of $\cos\theta^*_{Bosons}$.

invariant masses above 1300 GeV. The expanded bin widths were chosen at the tails of the distribution to ensure the bin contents are sufficiently well populated to make a reliable estimate the likelihood function using the χ^2 parameter. This choice of binning minimises the effect of large bin by bin fluctuations arising from individual events with large event weights.

Confidence limits describing the sensitivity of the CLIC experiment to the anomalous gauge couplings were found by examining this χ^2 surface in α_4 and α_5 space. Deviations about the minima of this surface, which by construction occurs at $\alpha_4 = \alpha_5 = 0$, yield confidence limits that indicate the probability of observing a particular value of α_4 and α_5. The confidence limits used in subsequent sections, 68%, 90% and 99%, are defined using fixed deviations from the minima of χ^2 contours of 2.28, 4.61 and 9.21 respectively. These numbers arise from the integral of the two dimensional χ^2 function.

It proved useful to consider the sensitivities to the individual parameters α_4 and α_5 independently. This was done by projecting out the $\alpha_4 = 0$ or $\alpha_5 = 0$ one dimensional χ^2 distribution from the two dimensional χ^2 as discussed in section 1.4.1. The sensitivity to individual parameters was then extracted using confidence limits arising from the integral of the one dimensional χ^2 function i.e. 68% confidence limit occurs for $\chi^2 = 0.989$. In subsequent chapters these are the sensitivities quoted for individual anomalous gauge couplings.

1.6.3 Event Weight Interpolation Scheme

As described in section 1.3, event weights are used to determine the sensitivity of CLIC to the anomalous gauge couplings. These event weights are extracted on an event by event basis for the signal final state $\nu\nu$qqqq from the generator Whizard. To achieve a smooth χ^2 distribution a fine sampling of the M_{VV} distribution in the α_4 and α_5 space is needed. However, as extracting the event weights is highly CPU intensive, it is unfeasible to produce a finely sampled grid of event weights on an event by event basis by calling the generator. To resolve this issue, an interpolation scheme was applied to determine the event weights within a sampled region of the α_4 and α_5 space. This allows for an infinite sampling of the M_{VV} distribution in the space of α_4 and α_5 within the sampled region, without having to call the generator an infinite number of times.

A bicubic interpolation scheme, cubic interpolation along two dimensions, was applied to the event weights that were extracted from the generator. This procedure is best illustrated by showing the interpolated surface superimposed with the raw event weights from the generator, which is shown for several $\nu\nu$qqqq events at 1.4 TeV in figure 1.11. This interpolation scheme produces a smooth and continuous surface that is sufficiently accurate for the fitting procedure applied in this analysis.

At 1.4 TeV event weights were produced from the generator, Whizard, by stepping along α_4 and α_5 in steps of 0.01 ranging from -0.07 to 0.07, as shown in figure 1.3. These range proved to be sufficient for the contours of interest for the CLIC sensitivity analysis at these energies.

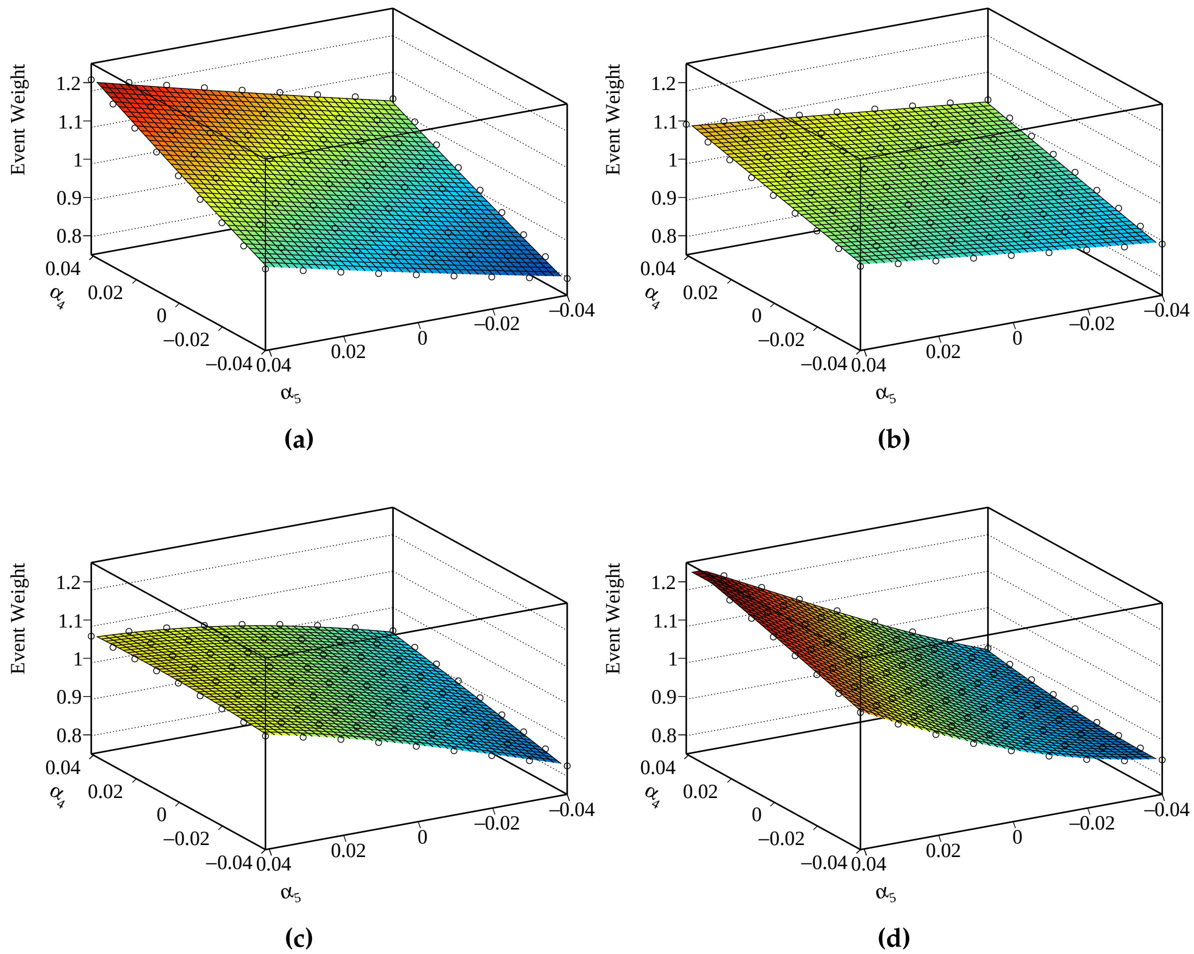

Figure 1.11: A selection of plots showing how the event weight changes when varying the anomalous couplings α_4 and α_5 for 1.4TeV $\nu\nu$qqqq final state events. The hollow circles show the event weight produced from the generator while the surface shown is found using bicubic interpolation between those points.

1.7 Results

The sensitivity of the CLIC experiment to the anomalous gauge couplings α_4 and α_5 at 1.4 TeV is shown in figure 1.12a. This result shows the sensitivity after the application of preselection and MVA described in sections 1.5.1 and 1.5.2 purposed to remove the included background channels, described in section 1.2. These contours yield the one σ confidence limit on the measurement of α_4 to the range -0.0082, 0.0116 and similarly for the measurement of α_5 to the range -0.0055, 0.0078.

1.7.1 Systematic Uncertainties

A source of systematic error in this experiment is the uncertainty on the cross sections for the signal and background final states. Based on the selection efficiencies given in table 1.4, the χ^2 fit procedure is applied on a distribution that primarily consists of the background final states qqqqν arising from the interaction of e^+ and e^+ with beamstrahlung photons. Therefore, uncertainties in the cross section for these backgrounds should be considered. A detailed study of the accuracy of the relevant cross section calculations has yet to be performed for CLIC and so a wide spectrum in the uncertainty of these cross sections is considered here.

This is systematic is included in the χ^2 through the use of a nuisance parameter, whereby the cross section for $\gamma_{\mathrm{BS}}\mathrm{e}^- \rightarrow \mathrm{qqqq}\nu$ and $\mathrm{e}^+\gamma_{\mathrm{BS}} \rightarrow \mathrm{qqqq}\nu$ are allowed to fluctuate. Assuming the cross sections are fluctuated by a factor r, the magnitude of the fluctuation is moderated by an additional penalty term in the χ^2 as follows:

$$\chi^2(r) = \sum_i \frac{(O_i - E_i(r))^2}{E_i(r)} + \frac{(r-1)^2}{\sigma_r^2} \tag{1.5}$$

where O_i is the observed, $\alpha_4 = \alpha_5 = 0$, bin content for bin i in the distribution of M_{VV} with no background fluctuations. $E_i(r)$ is the expected, $\alpha_4 \neq 0$ and $\alpha_5 \neq 0$, bin content for bin i in the distribution of M_{VV} with the $\gamma_{\mathrm{BS}}\mathrm{e}^- \rightarrow \mathrm{qqqq}\nu$ and $\mathrm{e}^+\gamma_{\mathrm{BS}} \rightarrow \mathrm{qqqq}\nu$ background cross sections fluctuated by the factor r. $\sum_i$ is the sum over the bins of the M_{VV} distribution and σ_r is the width of the distribution of r, which indicates the uncertainty on the measurement of the fluctuations and hence the background cross sections. The χ^2 surface is constructed in the space of α_4 and α_5 by minimising

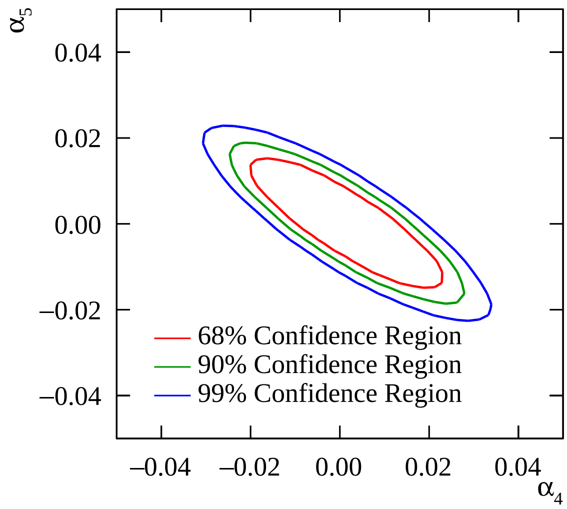

(a)

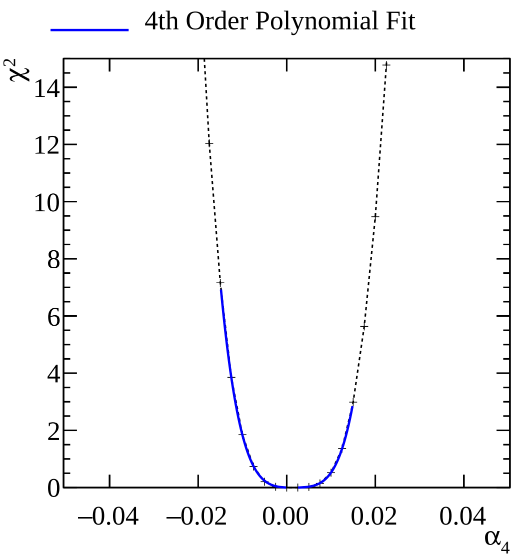

(b)

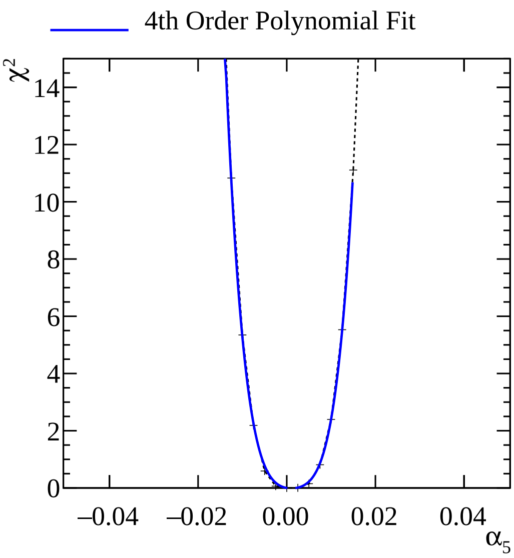

(c)

Figure 1.12: χ^2 sensitivity distributions from a fit to M_{VV} at 1.4 TeV. Results include the effect of backgrounds after the application of a series of preselection cuts and MVA. (a) χ^2 sensitivity contours in α_4 and α_5 space. (b) χ^2 as a function of α_4 assuming $\alpha_5 = 0$. (c) χ^2 as a function of α_5 assuming $\alpha_4 = 0$.

$\chi^2(r)$ at each point. The 68% confidence contour is shown with the inclusion of this nuisance parameter for various values of σ_r in figure 1.13.

Minimal changes in sensitivity are observed when allowing the backgrounds to fluctuate even up to the 50% level. This can be understood by considering the shape of the M_{VV} distribution for the signal, with and without the effect of anomalous couplings, and the $\gamma_{BS}e^- \rightarrow qqqq\nu$ and $e^+\gamma_{BS} \rightarrow qqqq\nu$ backgrounds, which is shown in figure 1.14. These distribution shows that anomalous couplings primarily affect events with large invariant masses, while the backgrounds peak at low invariant masses. Therefore, by fluctuating the cross-section for the background processes it is not possible to gain a better match between the observed and expected bin contents in the M_{VV} distribution. This is encouraging as despite these backgrounds dominating the fit being used to determine the sensitivity of CLIC to the anomalous gauge couplings, precise knowledge of their cross-section is not essential.

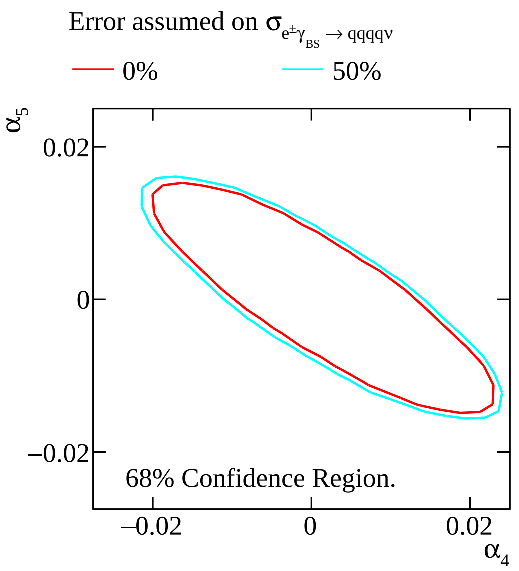

Figure 1.13: 68% sensitivity contour including systematic errors, of varying magnitudes, in dominant background cross sections.

1.8 Sensitivity at 3 TeV

The anomalous gauge coupling sensitivity study described in this chapter was reproduced for CLIC operating at 3 TeV. The procedure for the 3 TeV analysis largely mirrors that of the 1.4 TeV analysis, therefore in this section only the differences between the analyses are highlighted.

The signal and background final states for the 3 TeV analysis were identical to those used for the 1.4 TeV analysis as described in section 1.2. The cross sections at 3 TeV for those signal and background final states can be found in table 1.5. The data analysis

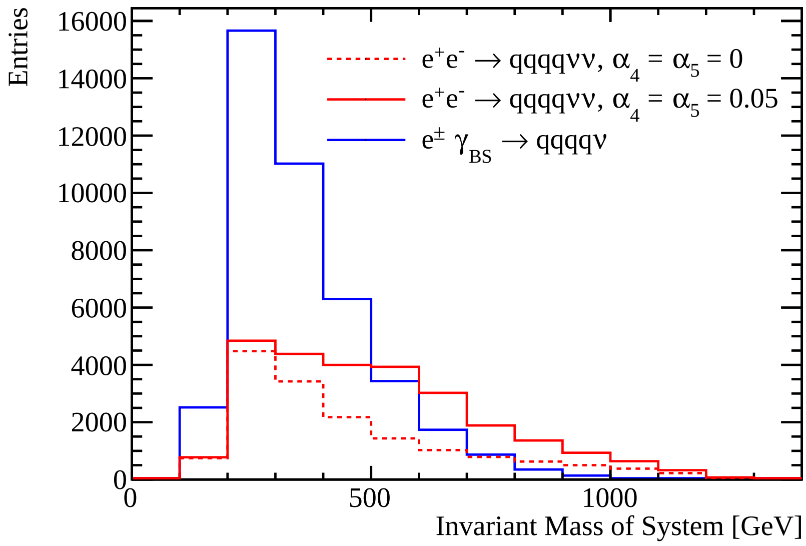

Figure 1.14: Distributions of M_{VV} for the $\nu\nu$qqqq, with and without the effect from anomalous couplings, and the combined dominant background processes $\gamma_{\mathrm{BS}}\mathrm{e}^- \rightarrow \mathrm{qqqq}\nu$ and $\mathrm{e}^+\gamma_{\mathrm{BS}} \rightarrow \mathrm{qqqq}\nu$.

and event selection procedures used at 3 TeV mirrored those used at 1.4 TeV. Detailed descriptions of both can be found in sections 1.4 and 1.5 respectively.

Jet finding was performed using the longitudinally invariant k_t algorithm as described in section . Optimisation of the jet algorithm configuration, which uses pure signal only as described in section 1.4.1, found the optimal configuration at 3 TeV to be tight selected PFOs and an R parameter of 1.1. As the cross section for the $\gamma\gamma \rightarrow$ Hadrons increases with energy the impact of this background is more problematic at 3 TeV than 1.4 TeV [10]. Therefore, it is to be expected that the optimal PFO selection at 3 TeV is more aggressive, tight selected PFOs, at vetoing these backgrounds than at 1.4 TeV, selected PFOs, which is what is observed.

The event selection for the 3 TeV analysis is summarised in table 1.6.

Due to the increased sensitivity of the signal sample at 3 TeV, the stepping along α_4 and α_5 to extract the event weights from the generator was much finer than that used for the 1.4 TeV analysis. At 3 TeV event weights were taken from the generator in steps of 0.00025 ranging from 0.0065 to -0.0065. Bicubic interpolation was again used to make a continuous surface for the event weights. These event weight surfaces were

Final State	Cross Section 3 TeV [fb]
$e^+e^- \to \nu\nu qqqq$	71.5
$e^+e^- \to l\nu qqqq$	106.6
$e^+e^- \to llqqqq$	169.3
$e^+e^- \to qqqq$	546.5
$e^+e^- \to \nu\nu qq$	1317.5
$e^+e^- \to l\nu qq$	5560.9
$e^+e^- \to llqq$	3319.6
$e^+e^- \to qq$	2948.9
$\gamma_{EPA}e^- \to qqqqe^-$	287.8
$\gamma_{BS}e^- \to qqqqe^-$	1268.6
$e^+\gamma_{EPA} \to qqqqe^+$	287.8
$e^+\gamma_{BS} \to qqqqe^+$	1267.3
$\gamma_{EPA}e^- \to qqqq\nu$	54.2
$\gamma_{BS}e^- \to qqqq\nu$	262.5
$e^+\gamma_{EPA} \to qqqq\nu$	54.2
$e^+\gamma_{BS} \to qqqq\nu$	262.3
$\gamma_{EPA}\gamma_{EPA} \to qqqq$	402.7
$\gamma_{EPA}\gamma_{BS} \to qqqq$	2423.1
$\gamma_{BS}\gamma_{EPA} \to qqqq$	2420.6
$\gamma_{BS}\gamma_{BS} \to qqqq$	13050.3

Table 1.5: The cross sections of signal and background processes at 3 TeV. In the above table q $\in$ u, $\bar{u}$, d, $\bar{d}$, s, $\bar{s}$, c, $\bar{c}$, b or $\bar{b}$ while l $\in e^{\pm}$, $\mu^{\pm}$ or $\tau^{\pm}$ and $\nu \in \nu_e$, ν_μ and ν_τ. The EPA and BS subscript on the incoming photon indicates whether the photon is generated from the equivalent photon approximation or beamstrahlung.

then used to construct the M_{VV} distribution and the χ^2 surface used to determine the reported sensitivities.

The sensitivity of the CLIC experiment to the anomalous gauge couplings α_4 and α_5 at 3 TeV is shown in figure 1.15a. This result shows the sensitivity after the application of preselection and MVA described in sections 1.5.1 and 1.5.2 purposed to remove the included background channels, described in section 1.2. These contours yield the one σ confidence limit on the measurement of α_4 to the range -0.0010 to 0.0011 and similarly for the measurement of α_5 the range is -0.0007 to 0.0007.

Final State	ϵ_{presel}	ϵ_{BDT}	N_{BDT}
$e^+e^- \to \nu\nu qqqq$	74.4%	46.0%	65,740
$e^+e^- \to l\nu qqqq$	40.0%	12.0%	25,660
$e^+e^- \to llqqqq$	7.5%	1.1%	3,570
$e^+e^- \to qqqq$	3.7%	0.3%	3,224
$e^+e^- \to \nu\nu qq$	50.5%	1.2%	30,510
$e^+e^- \to l\nu qq$	32.0%	0.4%	48,320
$e^+e^- \to llqq$	1.4%	-	1,028
$e^+e^- \to qq$	1.4%	0.1	3,268
$\gamma_{\text{EPA}}e^- \to qqqqe^-$	6.6%	0.8%	4,736
$\gamma_{\text{BS}}e^- \to qqqqe^-$	4.6%	0.7%	13,660
$e^+\gamma_{\text{EPA}} \to qqqqe^+$	6.5%	0.8%	4,686
$e^+\gamma_{\text{BS}} \to qqqqe^+$	4.7%	0.7%	13,310
$\gamma_{\text{EPA}}e^- \to qqqq\nu$	45.6%	17.2%	18,610
$\gamma_{\text{BS}}e^- \to qqqq\nu$	55.9%	26.7%	110,900
$e^+\gamma_{\text{EPA}} \to qqqq\nu$	45.9%	17.3%	18,750
$e^+\gamma_{\text{BS}} \to qqqq\nu$	56.5%	27.4%	113,700
$\gamma_{\text{EPA}}\gamma_{\text{EPA}} \to qqqq$	5.3%	0.7%	5,531
$\gamma_{\text{EPA}}\gamma_{\text{BS}} \to qqqq$	3.5%	0.4%	16,640
$\gamma_{\text{BS}}\gamma_{\text{EPA}} \to qqqq$	3.5%	0.4%	15,900
$\gamma_{\text{BS}}\gamma_{\text{BS}} \to qqqq$	0.6%	-	4,124

Table 1.6: Selection summary at 3 TeV. The EPA and BS subscript on the incoming photon indicates whether the photon is generated from the equivalent photon approximation or beamstrahlung. Cells omitting the efficiency indicate an efficiency of less than 0.1%.

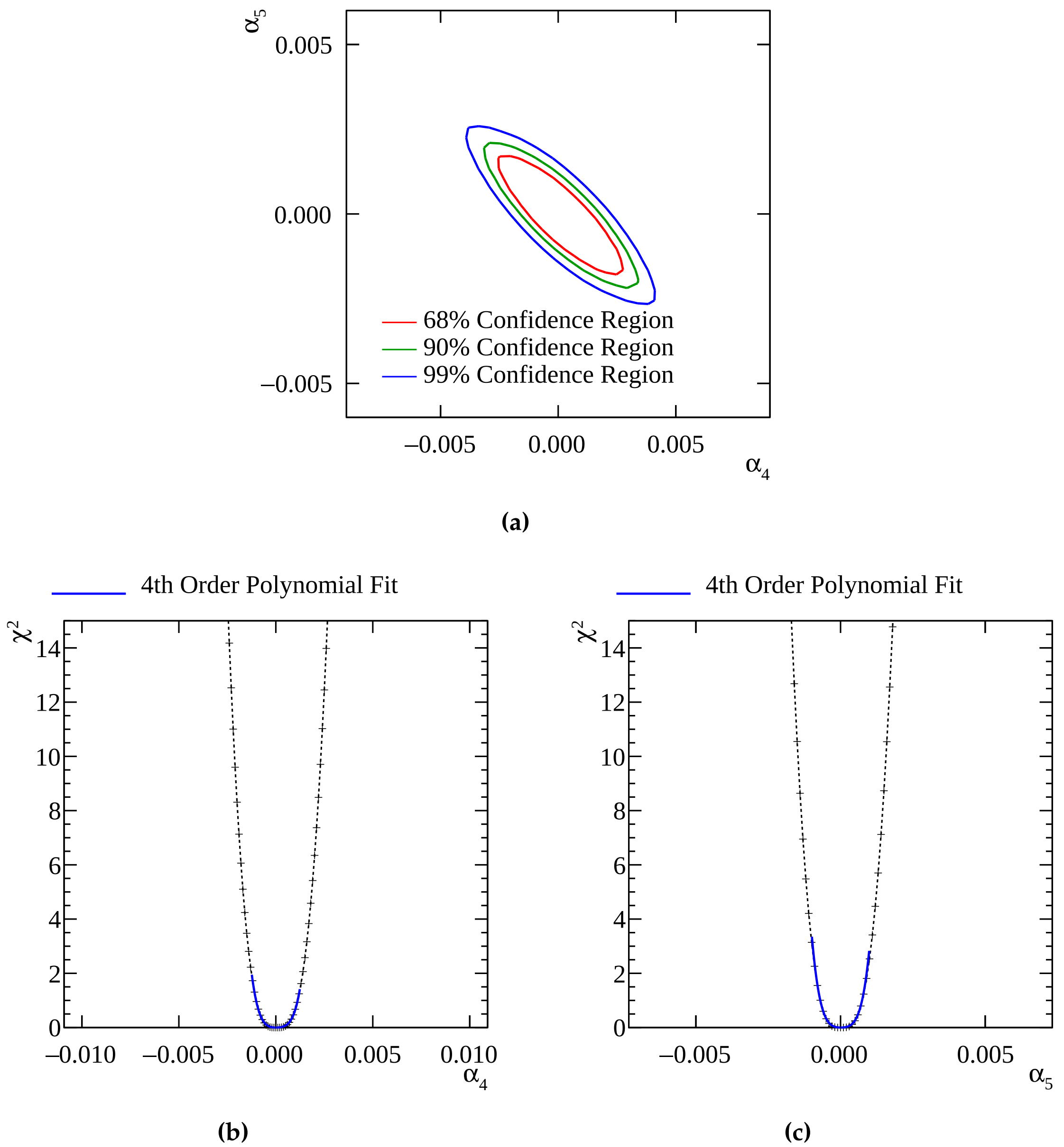

Figure 1.15: χ^2 sensitivity distributions from a fit to M_{VV} at 3 TeV. Results include the effect of backgrounds after the application of a series of preselection cuts and MVA. (a) χ^2 sensitivity contours in α_4 and α_5 space. (b) χ^2 as a function of α_4 assuming $\alpha_5 = 0$. (c) χ^2 as a function of α_5 assuming $\alpha_4 = 0$.

Colophon

This thesis was made in $\LaTeX\,2_\varepsilon$ using the “hepthesis” class [4].

Bibliography

[1] Toshinori Abe et al. The International Large Detector: Letter of Intent. 2010, 1006.3396.

[2] S. Agostinelli et al. GEANT4: A Simulation toolkit. *Nucl. Instrum. Meth.*, A506:250–303, 2003.

[3] J. Beringer et al. Review of Particle Physics (RPP). *Phys. Rev.*, D86:010001, 2012.

[4] Andy Buckley. The hepthesis LaTeX class.

[5] Matteo Cacciari, Gavin P. Salam, and Gregory Soyez. FastJet User Manual. *Eur. Phys. J.*, C72:1896, 2012, 1111.6097.

[6] F. Gaede. Marlin and LCCD: Software tools for the ILC. *Nucl. Instrum. Meth.*, A559:177–180, 2006.

[7] Andreas Hoecker, Peter Speckmayer, Joerg Stelzer, Jan Therhaag, Eckhard von Toerne, and Helge Voss. TMVA: Toolkit for Multivariate Data Analysis. *PoS*, ACAT:040, 2007, physics/0703039.

[8] Wolfgang Kilian, Thorsten Ohl, and Jurgen Reuter. WHIZARD: Simulating Multi-Particle Processes at LHC and ILC. *Eur. Phys. J.*, C71:1742, 2011, 0708.4233.

[9] Lucie Linssen, Akiya Miyamoto, Marcel Stanitzki, and Harry Weerts. Physics and Detectors at CLIC: CLIC Conceptual Design Report. 2012, 1202.5940.

[10] J. S. Marshall, A. MÃijnnich, and M. A. Thomson. Performance of Particle Flow Calorimetry at CLIC. *Nucl. Instrum. Meth.*, A700:153–162, 2013, 1209.4039.

[11] P. Mora de Freitas and H. Videau. Detector simulation with MOKKA / GEANT4: Present and future. In *Linear colliders. Proceedings, International Workshop on physics and experiments with future electron-positron linear colliders, LCWS 2002, Seogwipo, Jeju Island, Korea, August 26-30, 2002*, pages 623–627, 2002.

[12] Mauro Moretti, Thorsten Ohl, and Jurgen Reuter. O'Mega: An Optimizing matrix element generator. 2001, hep-ph/0102195.

[13] Torbjorn Sjostrand, Stephen Mrenna, and Peter Z. Skands. PYTHIA 6.4 Physics and Manual. *JHEP*, 05:026, 2006, hep-ph/0603175.

[14] M. A. Thomson. Particle Flow Calorimetry and the PandoraPFA Algorithm. *Nucl. Instrum. Meth.*, A611:25–40, 2009, 0907.3577.

[15] Z. Was. TAUOLA the library for tau lepton decay, and KKMC / KORALB / KORALZ /... status report. *Nucl. Phys. Proc. Suppl.*, 98:96–102, 2001, hep-ph/0011305. [,96(2000)].

List of figures

List of tables